



# A novel integrated approach of reactor network modeling for solar driven biomass pyrolysis process

Muhammad Ahsan Amjed<sup>a,b,\*</sup>, Marco Colombi<sup>b</sup>, Leon Loni Berkel<sup>c</sup>, Marco Binotti<sup>b</sup>, Matteo Carmelo Romano<sup>b</sup>, Tiziano Faravelli<sup>a</sup>

<sup>a</sup> Department of Chemistry, Materials, and Chemical Engineering, Politecnico di Milano, Piazza Leonardo da Vinci 32, 20133, Milano, Italy

<sup>b</sup> Department of Energy, Politecnico di Milano, Via Lambruschini 4, 20156, Milano, Italy

<sup>c</sup> Simulation of Reactive Thermo-Fluid Systems (STFS), TU Darmstadt, Otto-Berndt-Strasse 2, 64287, Darmstadt, Germany

## ARTICLE INFO

### Keywords:

Reactor network modeling  
Biomass pyrolysis  
Process modeling  
Fluidized bed reactor  
Solar driven pyrolysis

## ABSTRACT

Conventional pyrolysis of biomass is energy intensive and inefficient; direct solar pyrolysis faces issues such as non-uniform heating and limited control over process parameters. To address these challenges, indirect solar heating with particle heat carriers and thermal storage has been proposed, enabling continuous and efficient fast pyrolysis. Existing process modeling tools often oversimplify complex pyrolysis reactions, neglecting secondary reactions critical to predict yield accurately. This study introduces an advanced integrated reactor modeling framework using the NetSMOKE reactor network tool, capable of simulating fully coupled multiphase reactions, including devolatilization and gas-phase kinetics within a reactor block of process simulation. The model is validated against both experimental and computational fluid dynamics data, and it is integrated into a broader process simulation to predict product distributions across diverse feedstocks and operating conditions. The reactor network model achieves high accuracy with only a 0.1–3.4 percentage point error margin and marks the first application of such a fully coupled reactor model to biomass pyrolysis process. A comparison between the reactor network-based process model and the previous fixed Ryield-based model reveals a 4–10 percentage point difference in product yields. Furthermore, concentrated solar power (CSP) based pyrolysis demonstrates superior performance in both models, enhancing carbon efficiency (from 74.1–77.7 % to 90.7–92.9 %) and energy efficiency (from 73.9–75 % to 77.7–78.6 %), while significantly reducing the net emission to oil ratio (from 0 to –27.5/–35.8 kgCO<sub>2</sub>/GJ<sub>oil</sub>), highlighting clear environmental and performance benefits. A sensitivity analysis was also performed to assess the influence of operating temperature on product distribution, efficiencies, and carbon emissions.

## 1. Introduction

Biomass is one of the renewables with a wide potential for future energy security and climate mitigation due to its carbon-neutral nature [1]. There are huge biomass residues from forestry, municipal, food industry and agricultural waste that would be dumped on land or often burned in the open air in developing nations resulting in severe environmental pollution. By 2050, biomass could supply 3000 TWh of electricity and reduce emissions by 1.3 Bt CO<sub>2</sub> equivalent per year, while producing 472.9 Kt CO<sub>2</sub> for every one TWh of energy generated [2]. Among thermochemical conversion methods, pyrolysis is widely used; it heats biomass in the absence of oxygen, where feedstock decompose into

gaseous, liquid (bio-oil), and solid (char) products [3].

Conventional biomass pyrolysis, an inherently endothermic process, requires substantial thermal energy to maintain reactor operation, leading to reduced energy efficiency and increased carbon emissions [3]. To overcome these limitations, various researchers [4–10] have explored solar assisted pyrolysis at the laboratory scale, employing direct reactor radiative heating using Fresnel lenses or parabolic concentrators. However, the direct heating with concentrated solar power (CSP) encounters several challenges, including non-uniform temperature profiles within the reactor, thermal stress due to fluctuating solar irradiance, and lower bio-oil yields resulting from slow pyrolysis kinetics. Additionally, the difficulty of temperature and heating rate

\* Corresponding author at: Department of Chemistry, Materials, and Chemical Engineering, Politecnico di Milano, Piazza Leonardo da Vinci 32, 20133, Milano, Italy.

E-mail addresses: [muhammadahsan.amjed@polimi.it](mailto:muhammadahsan.amjed@polimi.it), [m.ahsanamjed@gmail.com](mailto:m.ahsanamjed@gmail.com) (M.A. Amjed).

<https://doi.org/10.1016/j.cej.2025.172206>

Received 15 September 2025; Received in revised form 4 December 2025; Accepted 22 December 2025

Available online 5 January 2026

1385-8947/© 2025 The Authors. Published by Elsevier B.V. This is an open access article under the CC BY license (<http://creativecommons.org/licenses/by/4.0/>).

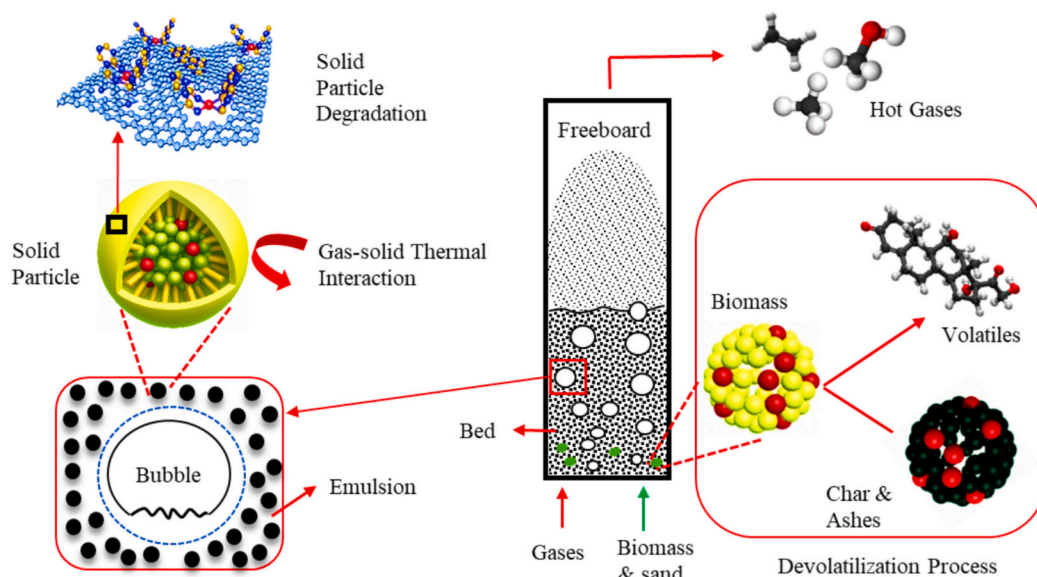


Fig. 1. Biomass thermochemical degradation and fluidization process in fluidized bed reactor.

control related to the intermittent nature of solar irradiation, restricts its practical application [3,9].

Indirect solar heating of pyrolysis reactor using a heat transfer medium can mitigate these issues, also enabling integration with thermal energy storage for continuous operation. Molten salts provide stable, high capacity, heat transfer and can supply heat to pyrolysis reactor externally [11,12] or by direct mixing with biomass [13]. External circulation through heat exchangers works at small scale but scaling up external molten salt heating may face issues of uneven temperature distribution in the reactor, increased fouling, risks of salt solidification, pressure drop, and system complexity of secondary heat exchange [14]. Direct mixing improves internal heat transfer but introduces challenges such as biochar contamination, difficult solid liquid separation, possible salt degradation or fouling, and higher corrosion risks [15]. PHCs have also been investigated as both heat transfer media and fluidized bed materials, enabling efficient heat delivery from solar plants to pyrolysis reactors. Although still under development and facing heating rate control challenges, the Horizon Europe PYSOLO project [16] is advancing PHC based CSP systems [17], which aim to enhance overall energy and carbon efficiency while supporting continuous plant operation through integration with thermal energy storage.

Beyond the inherent challenges of energy efficiency and carbon emissions in conventional biomass pyrolysis, a significant limitation lies in the inadequate representation of the pyrolysis reactor within existing process modeling tools. Several studies presented in literature analyze biomass pyrolysis and gasification using process simulators such as Simulink [18], Aspen Plus® [17,19–21] and Cycle Tempo [22], effectively analyzing energy and mass balances for subsequent economic, environmental, and life cycle assessments [17,20], but they falling short in accurately capturing the complex nature of the pyrolysis process itself. Process simulators like Aspen Plus® offer reactor components for biomass pyrolysis simulation, they lack the necessary flexibility for comprehensive analysis. For example, the fixed yield pyrolysis reactor models, as utilized by Amjed et al. [17], cannot account the variability of diverse biomass feedstocks or the impact of operating parameters on product composition. Critically, they fail to represent detailed reaction pathways and the formation of intermediate species, leading to deviations between model predictions and experimental data [17,19,20].

The heart of the pyrolysis process is the reactor, which determine the oil and char yield and as well as their quality and accounts for 10–15 % of total capital investment [23]. Fig. 1 provides a visual representation of the various processes within a fluidized bed for biomass pyrolysis.

These include heat exchange between solids and gases, gas diffusion to solids and solid degradation to char and volatiles. To understand these complex processes, engineers typically break them down into three key sub-models such as fluid dynamics, chemistry, and heat transfer. These processes are strongly interlinked and influence each other significantly. This strong interlink makes challenging to solve the overall behavior of the fluidized bed [24].

While experimental studies are valuable for examining how various parameters influence pyrolysis performance, they are costly, operationally complex, and typically limited to lab or pilot scale systems [25]. Mathematical modeling therefore becomes essential for analyzing the highly complex phenomena involved in biomass pyrolysis in fluidized bed reactor [26]. Numerous models have been developed to address the complex hydrodynamic, thermodynamic, and chemical phenomenon in these reactor [26–28]. However, because biomass pyrolysis is a multi-scale, multi-step, multi component and multi-phase process, creating a single model that captures detailed reactor scale hydrodynamics along with kinetics and transport phenomena remains extremely difficult [27]. Computational fluid dynamics (CFD) offers detailed and accurate hydrodynamic predictions, but incorporating full reactive flows with detailed kinetics remains computationally demanding, restricting its use to simplified kinetics mechanisms [29–31].

Besides this, the reactor network modeling framework use the network of ideal reactors to capture hydrodynamics as mixed and streamlined flows and can use detailed chemical kinetics. One of the earliest modeling works based on the reactor network concept and detailed kinetic mechanisms was presented by Ehrhardt et al. [32] for modeling of NO<sub>x</sub> formation in a pilot-scale furnace. CFD with a very simplified kinetic mechanism was applied to map zones bounded by streamlines and axial components. Then, the reaction progress in each ideal reactor representing these zones was calculated using a detailed kinetic mechanism. Falcitelli et al. [33], developed and studied an algorithm that can extract reactor networks from industrial CFD simulations of combustion processes. A recent novel approach by Trespi et al. [34] employed a combined equation oriented and sequential modular method to solve the global equation system of the reactor network, validated against oxy fuel combustion experiments. Among the reviewed works, Darido et al. [35] modeled a domestic wood combustion unit by simulating the pyrolysis in a separate perfectly stirred reactor (PSR), and the subsequent secondary gas phase reactions in a series of PSR and plug flow reactors (PFR) network. In a slightly different approach by Das et al., [36] the thermodynamic equilibrium model is

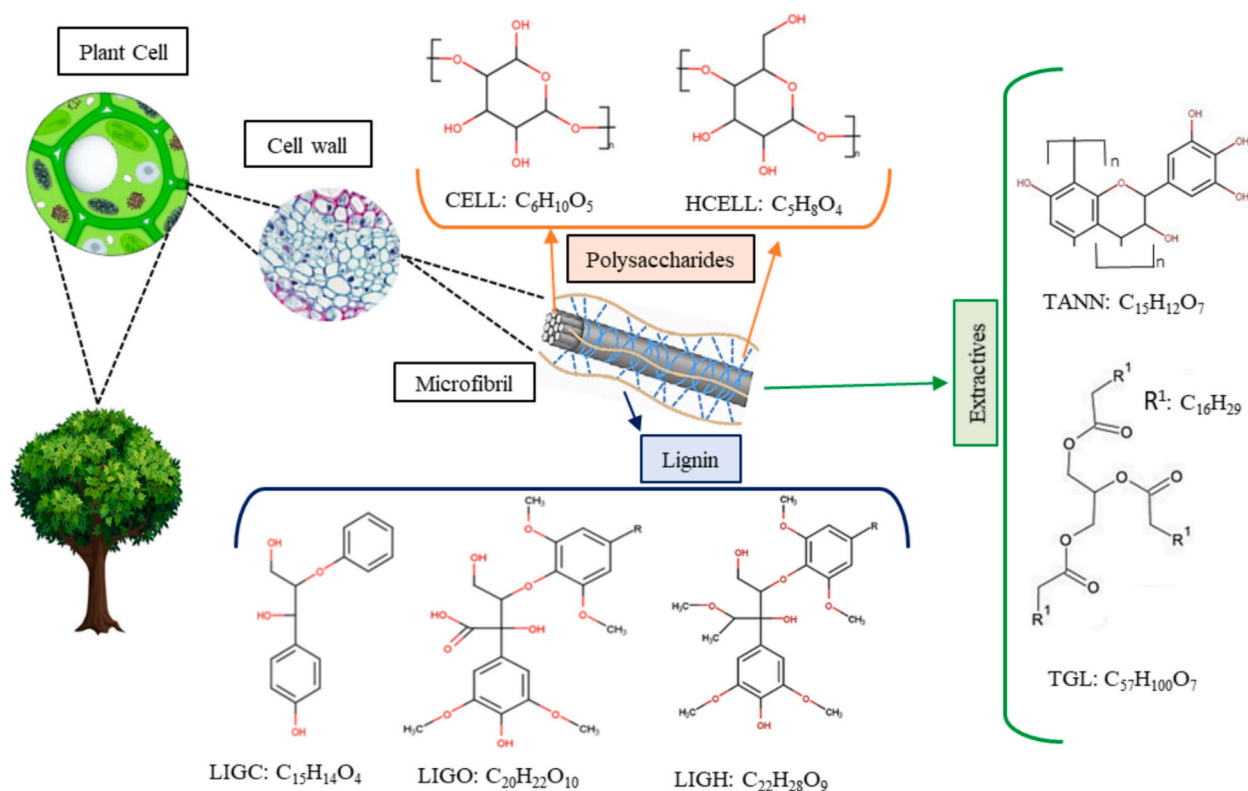


Fig. 2. Biomass characterization and reference species used in CRECK-S-B model-inspired from [40].

coupled with the reactor network model. In this approach, gas phase species are generated from the thermodynamic equilibrium and fed to a simple reactor network consisting of a PSR representing the pyrolysis in the bed and a PFR representing the freeboard.

Further progress has been made by Stark et al. [37] by incorporating a one dimensional particle model to capture the particle devolatilization and the resulting gas species are fed to a gas-phase reactor network. All of those discussed in previous works fail to consider the simultaneous nature of devolatilization and gas phase reactions. CRECK modeling group developed a tool (NetSMOKE) to solve a complex reactor network in which a multiphase (gas and solid) flow reactor was applied for biomass gasification [38] having the ability to deal with fully coupled heterogeneous reactions. This model shows its ability to solve complex reactor networks computationally in a quick and efficient way.

Building on this foundation, the NetSMOKE tool demonstrates strong capabilities in handling complex reactor configurations and detailed chemical kinetics for multiphase biomass pyrolysis. However, it lacks the necessary auxiliary process components to perform comprehensive mass and energy balance calculations for the analysis of entire process. In contrast, process simulators such as Aspen Plus® are well equipped to conduct full process analyses, including mass and energy balances, economic evaluation, and environmental assessments, but they do not provide detailed reactor level descriptions or accommodate complex pyrolysis kinetics effectively. Additionally, introducing detailed kinetic mechanisms directly into Aspen Plus® is both technically and computationally challenging. The integration of the reactor network (RN) approach implemented in NetSMOKE within Aspen Plus® using Fortran subroutine offers a promising solution to overcome these limitations by combining the strengths of both tools. This integrated modeling framework significantly enhances the accuracy, robustness and flexibility of biomass pyrolysis process simulations, enabling improved prediction of product yields and compositions across diverse feedstocks and operating conditions.

This study, part of the PYSOLO project [16], builds upon and extends

our previous studies [17,38] by applying and validating the proposed NetSMOKE reactor network model for biomass pyrolysis in a fluidized bed reactor. In this study, the validated reactor network model is eventually integrated with a comprehensive biomass pyrolysis process model developed in [17] to enhance its flexibility, enabling the prediction of product compositions under a wide range of feedstocks and operating conditions. To the best of the authors' knowledge, this is the first application and integration of a fully coupled, multiphase reactor network approach to industrial scale biomass pyrolysis process model.

The work is structured as follows: Chapter 2 outlines the modeling approach and its validation using three literature cases; two supported by CFD simulations for temperature and velocity profiles, and a third relying solely on experimental data, taking advantage of the first two cases. Chapter 3 compares conventional and solar-assisted pyrolysis processes, while Chapter 4 details the integration of the reactor network model with a commercial process simulation tool to enhance output predictivity. Chapter 5 evaluates the integrated model using key performance indicators and compares it to simplified fixed yield reactor models. Finally, Chapter 6 explores how efficiencies, emissions, and process parameters respond to temperature variations through sensitivity analysis.

## 2. Fluidized bed reactor model

Before using the reactor network model in the process analysis, we briefly present the main features of the approach and its validation, to show its reliability in comparison with a few experimental data from the literature.

### 2.1. Biomass characterization and chemical kinetics

To model the thermochemical conversion process, it is necessary to precisely describe the chemical composition of biomass and chemical reactions involved in the process. When direct biochemical composition

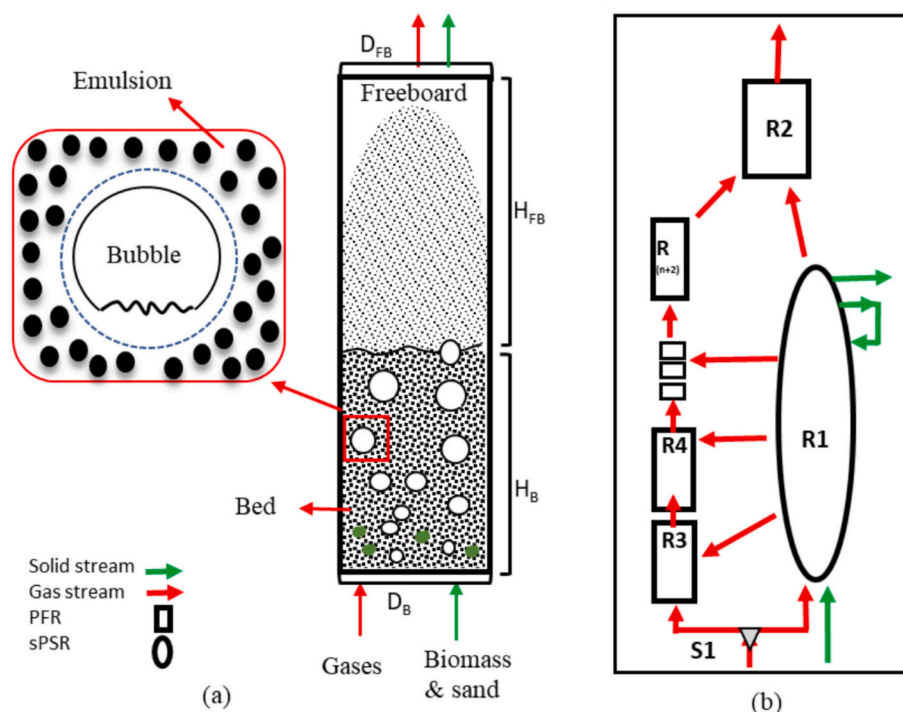


Fig. 3. (a) The schematic diagram of the bubbling fluidized Bed reactor (b) the reactor network map -adapted from [38].

of biomass is unavailable, elemental analysis can be used to derive this composition. This approach, adapted from Ranzi et al. [27], relies on H/C/O atomic balances to determine an appropriate combination of CRECK reference species. To model biomass pyrolysis kinetics, the CRECK-S-B model was selected because it offers a detailed, chemical kinetic representation of primary and secondary pyrolysis pathways, including tar formation and gas phase reactions. Compared with lumped or global kinetic models, CRECK-S-B provides higher accuracy across a wide range of variable operating conditions and has been extensively validated in previous studies [38–43]. This makes it well suited for CFD and reactor scale simulations requiring reliable prediction of product distribution and reaction behavior.

In plant cell walls, microscopic cellulose microfibrils are embedded in a supportive matrix of hemicellulose and lignin; to simplify this complex structure, the CRECK model characterizes biomass by lumping these components into three categories: polysaccharide (cellulose and hemicellulose), Lignin and extractives (Fig. 2). The linear combination of these species in various proportions and their devolatilized profiles help to characterize and predict thermochemical conversion of wide range of biomasses. The amount of reference species is based on the elemental composition of the specific biomass type. From above mentioned categories, Cellulose (CELL) represents the monomer anhydrous glucose in biomass, while hemicellulose (HCELL) is represented by two reference species, GMSW (from softwood) and XYHW (from hardwood), having similar molecular structure but separate reacting path.

Lignin is characterized in three types of pseudo aromatic monomers based on their chemical composition (LIG—C, LIG—H and LIG—O). Similarly, TGL and TANN represent the hydrophobic and hydrophilic extractives in biomass feed, respectively. The characterization procedures and kinetic model details are explained in Debiagi et al. [40,41]. For gas phase, the CRECK-G-B kinetic model is employed: it is a detailed mechanism of 626 species, including all the species released from solid biomass phase, and 21,732 reactions [44].

## 2.2. Reactor network generation for fluidized bed reactor

The reactor networks to represent fluidized bed reactors are built and

solved via NetSMOKE, a numerical framework for solving and analyzing complex reactor networks with arbitrary interconnections [38]. The reactor network (RN) model is adopted from our recent study [38] where the model development, solution algorithms and employed fluidization correlations are already explained in detail.

In general, an arbitrary flow field can be represented with a network of ideal reactors by categorizing the whole domain mainly into two types of regions: regions with straight flows without back mixing are represented with PFRs, while regions with strong recirculation/mixing are represented with PSRs. Furthermore, the residence times, temperatures and flow rates of each compartment (ideal reactor unit within the RN) are required to fully characterize the RN. When available, these information can be obtained from CFD models as described in [34]. To describe a RN in NetSMOKE, each unit within the RN is connected via streams. These interconnecting streams distribute the mass flows among ideal reactor units with the help of splitter and mixer units. The residence time (or volume) and temperature must also be defined for each of the ideal reactor units. All this information as well as the mass flow rate and composition of the inlet streams to the system must be described in an input file. Arbitrarily complex RNs can be created with this approach.

For a fluidized bed reactor (or other configurations with known hydrodynamic behavior) generic flow structures can usually be assumed, and empirical correlations can be used for approximating residence times without necessarily having a prior CFD simulation. For a bubbling fluidized bed, Davidson's approach [45] describes three major regions, illustrated in Fig. 3a: the bubbles, the freeboard above the bed and the emulsion phase in the bed region. The emulsion phase consists of tightly packed solid particles and interstitial gas that are mixed well. In contrast, the bubble region is assumed to contain negligible amounts of solids, with gas moving upward through the bed. All gases from both the bubbles and the emulsion eventually rise and are found in the region above the bed (usually called the freeboard) during the experiment. These regions and their representation in a RN with ideal reactors are shown in Fig. 3b. The emulsion phase, freeboard, and the bubbles are represented by ideal reactors R1, R2 and R3 (and possibly more reactors to represent bubbles with R4, R5 ... R(n + 2) where n is the number of reactors to represent the bubble region), respectively. The split of mass



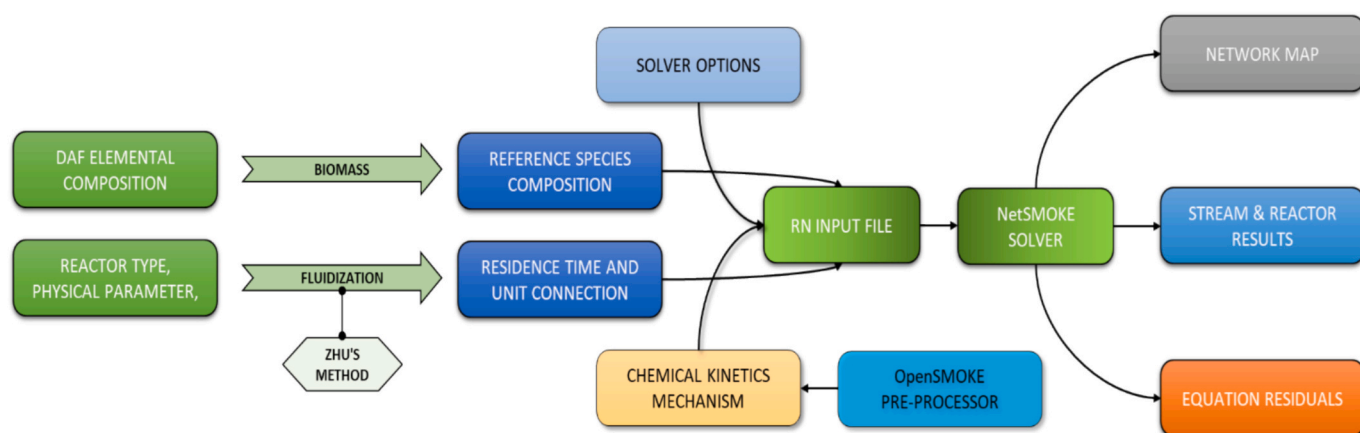


Fig. 4. The process flowchart of the proposed NetSMOKE reactor network tool for fluidized bed reactors- adapted from [38].

flowrates between the bubble and emulsion, as well as the residence times of these regions can be estimated by empirical correlations [46]. Similar approaches have been used in previous reactor network studies [37,47]. Further details of the approach can be found in [38], where the procedure is automatized and implemented in NetSMOKE based on the geometrical features of the system and operating conditions. In the current work, residence time information from CFD and experimental studies are used.

In the emulsion phase discussed above (represented with R1), both gas and solid reactions occur simultaneously. To account for this, a solid-gas PSR (sPSR) model has been developed in [38] to solve both phases in a fully coupled manner, and can be generally used to represent regions with strong solid-gas mixing. Similar to the gas-phase PSR, sPSR is also zero-dimensional reactor with infinitely fast mixing. The main assumptions considered in this model are:

- Solid and gas phases mix perfectly, and occupy separate volumes within the sPSR
- Transport between solid particles and gas phase are instant, without diffusion limitations
- Solid and gas phase species have the same residence time.

These assumptions capture the behavior where the chemical reaction is the rate limiting step and the solid particles are fully entrained in the gas flow. However, the solid product at the outlet of sPSR can be recycled and fed again at inlet of the same sPSR within the reactor network, increasing the total reaction time for solids compared to gas phase.

The process flowchart of NetSMOKE is summarized in Fig. 4. For a fluidized bed reactor, firstly, the RN input file is created with the algorithm described above. The reactor's height ( $H_{FB}$  and  $H_B$ ) and diameter ( $D_{FB}$  and  $D_B$ ) as illustrated in Fig. 3a, along with the operating pressure and temperature, the properties of the solid and gas phases, and the fluidization properties of the material. The desired number of PFRs required to represent the bubble region is specified using an additional parameter called 'n'. As a result, a network is automatically generated which is described in the RN input file, as given by Fig. 4. Afterward, the network is solved to obtain the outlet composition predictions by using the algorithm explained in [38]. The automatically generated RN input file can also be manually adjusted for more detailed analysis if required. After the solution of the RN, the properties of each stream and reactor, the residuals of the solved equations and a visual network map showing the topology of the RN under consideration are obtained.

### 2.3. Model validation

The reactor model is applied and validated on 3 different biomass pyrolysis case studies in which two of them include CFD simulations of

Table 1  
Selected case studies definition for the model validation.

Parameter	Case study 1	Case study 2	Case study 3
References	Lu et al., 2021 [43]	Lu et al., 2022 [48]	Tran et al., 2021 [49]
Study type	CFD	CFD + Experimental	Experimental
Biomass type	Loblolly pine wood	Bark of pine wood	Pitch pine wood
Reactor diameter (cm)	5.25	5.25	3.3
Reactor height (cm)	43.1	43.1	50
Reactor temperature (°C)	467.4, 468.7, 470.0	500	400, 450, 500, 550
Biomass feed rate (kg/h)	0.425	0.15	0.1
Biomass initial temp (°C)	25	25	25
Inlet gas Type	Nitrogen	Nitrogen	Nitrogen
Gas flow rate (kg/h)	1.0512	1.156	1.125
Bed material	Sand	Sand	sand
Particle size (mm)	0.13, 0.248, 0.40	1	0.55
Mean residence time (s)	4.27, 6.72, 14.32	10.43	3

Table 2  
Biomass characterization of loblolly pine wood [wt. fraction] [43].

Ref. Species	Wt. frac.	Ref. Species	wt. frac.	Ref. Species	wt. frac.
CELL	0.3754	LIGH	0.1679	TGL	0.0531
GMSW	0.2326	LIGC	0.0000	Moisture	0.0604
LIGO	0.1060	TANN	0.0000	Ash	0.0046

the fluidized bed reactor (FBR) and one is purely experimental. The key information about the selected cases studies is reported Table 1.

#### 2.3.1. Case study 1

Lu et al., 2021 [43] conducted a CFD simulation study on biomass pyrolysis and compared its findings with the experimental results. The pyrolysis of loblolly pine wood is analyzed in a bubbling fluidized bed reactor (BFBR) of 5.25 cm of diameter, 43.1 cm of height and at constant wall temperature of 500 °C, maintained using a heat jacket. The flow rate of loblolly pine biomass entering the BFBR is 0.425 kg/h at temperature of 25 °C and the total flow rate of hot nitrogen gas entering the BFBR is 1.0512 kg/h at 500 °C. The bed of the BFBR is composed of 330 g sand particles, which have 2500 kg/m<sup>3</sup> of initial density while biomass particles have 540 kg/m<sup>3</sup> of initial density.

In this CFD study, CRECK kinetic scheme [41] is used and biomass is already defined in term of reference species (cellulose, hemicellulose,

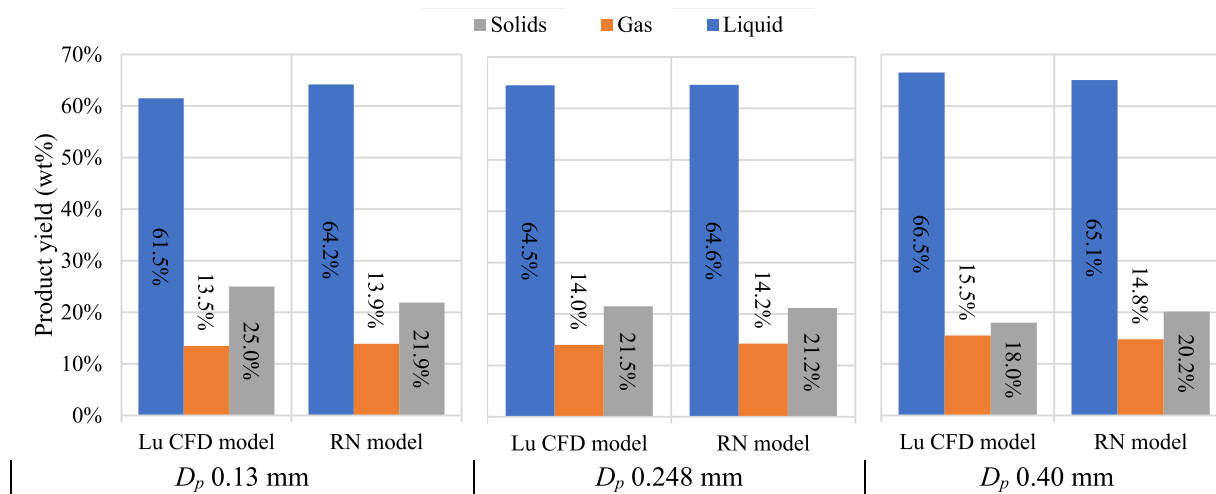


Fig. 5. The product yield comparison of Lu CFD with NetSMOKE model at various biomass particle sizes.

lignin etc.). Table 2 also reports the weight percentage of reference species and characterization of the loblolly pine wood biomass feed.

The bed consists of inert sand and loblolly pine biomass particles, with three different biomass particle sizes ( $D_p$ ) examined: 0.130 mm, 0.248 mm, and 0.400 mm. Simulations were performed using a coarse-grained CFD-DEM (discrete element method) approach that accounts for gas-solid hydrodynamics, interphase mass and heat transfer, and pyrolysis kinetics.

The mean residence times of biomass particles in the reactor increased with size, measured at 4.27 s for 0.130 mm particles, 6.72 s for 0.248 mm particles, and 14.32 s for 0.400 mm particles. Correspondingly, the average biomass particle temperatures were 467.4 °C, 468.7 °C, and 470.0 °C, respectively. These residence time values and their size dependence were obtained from the CFD study of Lu et al., 2021 [43], who reported that larger particles exhibit longer residence times due to their higher terminal velocities and reduced tendency to be elutriated from the bed. Furthermore, larger biomass particles heat more slowly and undergo pyrolysis at a reduced rate, which delays their density reduction and prolongs their retention within the reactor.

In the RN models, the corresponding mean residence times and average temperatures with respect to each particle size were applied for comparison (Fig. 5). The default splitting ratio of 99 % is used for solid recirculation to sPSR within reactor network. The parameters and auxiliary units used to develop RN input file are provided in supplementary information section S.1. The reactor network model generated for validation comprises only one bubble region ( $n = 1$ ) (Fig. 3 b). The results of the RN NetSMOKE model (Fig. 5) show satisfactory agreement with the Lu CFD model, with differences in solid and liquid product yields between 0.1 and 3.1 percentage points. Notably, the gas yield predictions are the most accurate, with a minimal deviation of only 0.25 to 0.71 percentage points compared to the CFD results, highlighting the RN model's strong capability in predicting yield of pyrolysis in BFBR. The RN model accurately follows the yield trend.

As the biomass particle size increases (from left to right in the Fig. 5), there is a clear increase in liquid and gas yields and a corresponding decrease in solid yield. This behavior can be explained by the longer residence time that larger biomass particles experience within the pyrolysis reactor, allowing more time for thermal decomposition. The extended residence time enhances the conversion of solid residues into volatiles, thereby increasing the production of liquid and gas products.

### 2.3.2. Case study 2

In another study, Lu et al. [48] conducted a multiscale CFD simulation of biomass feedstocks and compared it with the experimental data. The bark of pine wood is selected for comparison of the CFD and

Table 3

Biomass characterization of bark wood [wt%] [48].

Ref. Species	wt%	Ref. Species	wt%	Ref. Species	wt%
CELL	0.2932	LIGH	0.0000	TGL	0.0312
GMSW	0.2148	LIGC	0.3284	Moisture	0.0586
LIGO	0.0000	TANN	0.0668	Ash	0.0069

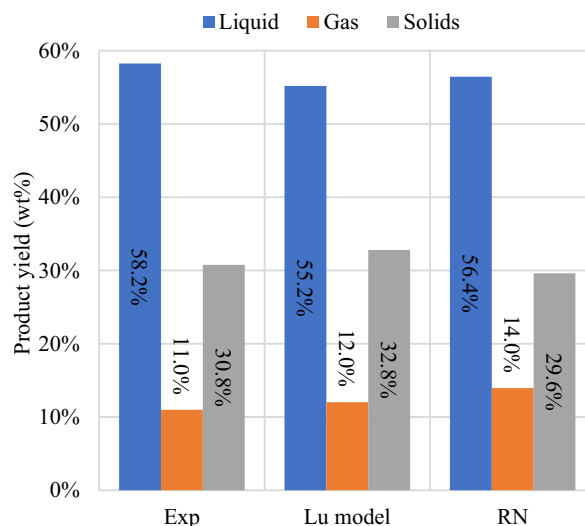


Fig. 6. The overall product yield comparison of Lu model and proposed RN model.

NetSMOKE results among other various feedstock types. BFBR has similar geometry to that used in previous case study [43]. The flow rate of bark wood biomass is 150 g/h at initial temperature of 25 °C, while the total flow rate of nitrogen gas is 0.3212 g/s at 500 °C. The bed of the BFBR is composed of 330 g of sand while the initial density of sand and biomass is 2500 kg/m<sup>3</sup> and 457 kg/m<sup>3</sup> respectively.

Table 3 reports the weight percentage of reference species and characterization of the bark wood biomass feed, which is characterized by using CRECK model [41]. The mean residence time for bark wood (10.4 s) calculated in CFD simulations is used in NetSMOKE model. Similar to the first case, a simplest RN model ( $n = 1$ ) is taken for comparison in which one sPSR represents the emulsion region, one PFR as bubble region and one PFR as free board for gases.

**Table 4**

Proximate and ultimate analysis of pitch pine tree [49].

Parameters	PA [wt%, dry basis]	Parameters	UA [wt%, DAF basis]
Moisture	6.90	C	50.28
Ash	0.30	H	6.18
Volatile	78.69	O	43.46
Fixed Carbon	14.84		

**Table 5**

Biomass characterization of pitch pine tree obtained from CRECK-S-B model [wt %].

Ref. Species	wt%	Ref. Species	wt%	Ref. Species	wt%
CELL	0.4242	LIGH	0.0805	TGL	0.0186
GMSW	0.2026	LIGC	0.1324	Moisture	0.0690
LIGO	0.0288	TANN	0.0409	Ash	0.0030

The experimental data provided by Lu et al. [48] has 3.7 % experimental mass error and normalized values of overall yield are taken for comparison. The developed reactor network model (RN) has almost the same overall product yield, using same operating conditions and initial chemical composition of feedstock. In this case study, the overall yield results of solids and liquid (Fig. 6) in the proposed RN model are closer to the experimental data compared to the Lu CFD model, with only a small difference of about ~1–2 % points, demonstrating the accuracy of the NetSMOKE model. However, the gas yield in the RN model is slightly higher than the experimental value, with a difference of approximately 3 percentage points.

### 2.3.3. Case study 3

Tran et al. [49] conducted a pyrolysis experiment in a bubbling fluidized bed reactor (BFBR) to investigate the pyrolysis of pitch pine wood. The BFBR used in the experiment had a diameter of 3.3 cm and a height of 50 cm. The reactor was operated at four different temperatures: 400 °C, 450 °C, 500 °C, and 550 °C, with a biomass feed rate of 100 g/h. The minimum fluidization velocity of nitrogen gas introduced from the bottom of the reactor was 5 L/min. Although Tran et al. studied various nitrogen flow rates, for this analysis, a gas flow rate three times the minimum fluidization rate was selected, using biomass particles with a diameter of 0.55 mm. The proximate and ultimate analyses of the biomass are presented in Table 4.

The characterization of pitch pine wood is done by using CRECK-S-B model [41] and the reference species of the biomass is reported in

**Table 5.**

The experimental residence time is almost 3 s and same residence time is considered in RN model. A comparison (Fig. 7) shows that the difference of overall yield from the experimental results is very small from NetSMOKE model, which varies from 0.1 to 3.4 % points.

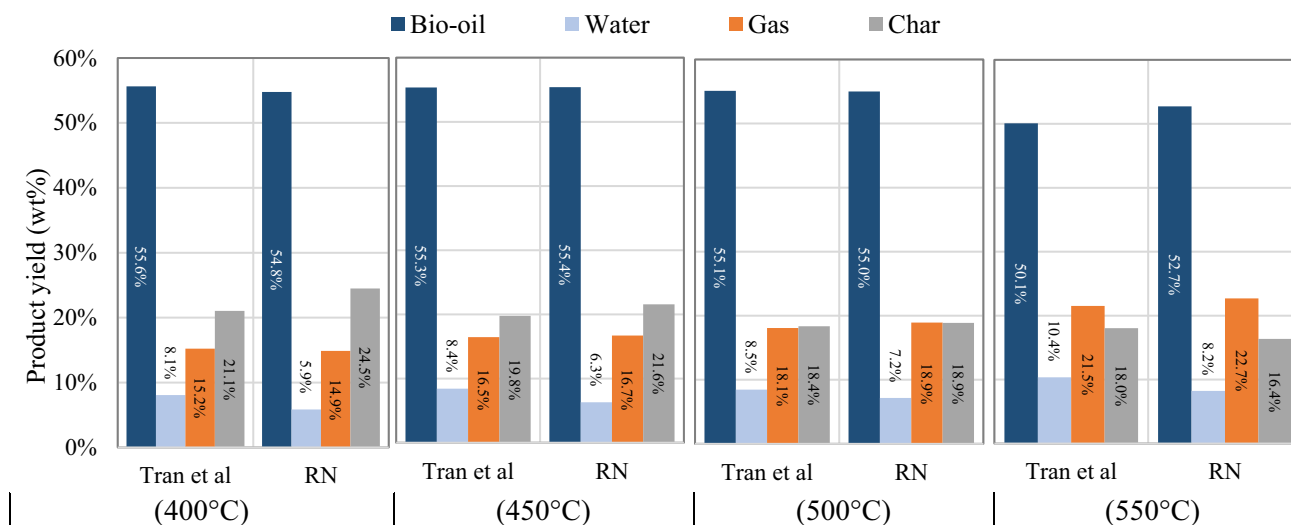
The RN model accurately reflects the yield trends reported by Tran et al. [49] across varying pyrolysis temperatures. As temperature increases (left to right in the Fig. 7), gas and water yields rise, while bio-oil slightly decreases and solids decline moderately. This trend is consistent with pyrolysis kinetics, where higher temperatures enhance secondary cracking and decomposition, converting more vapors and solids into non-condensable gases and water. The observed decline in bio-oil yield at higher temperatures can be attributed to the thermal cracking of larger organic liquid molecules into lighter, non-condensable gaseous products.

The small error range (0.1–3.4 %) observed between the reactor network model predictions, CFD simulations, and experimental data can be attributed to several factors. These include inherent simplifications in the reactor network approach, difference in kinetic parameters, and experimental measurement errors. Additionally, limitations in fully capturing complex secondary reactions and gas phase chemistry may also contribute to these discrepancies. Despite these factors, the low error margin confirms the model's reliability and effectiveness for accurate and efficient pyrolysis process simulation.

Computational fluid dynamics (CFD) models are important for the development of the reactor models and help to analyze the detail profile of flows, temperature and physical changes throughout the reactor. CFD provides a highly resolved hydrodynamic profile in the design of a pyrolysis reactor.

However, handling detailed chemical kinetics remains computationally very challenging. Biomass pyrolysis and similar multistep reacting systems require hundreds of species and thousands of reactions, which can make CFD simulations extremely stiff, slow, and difficult to converge. This limitation is especially pronounced when multiple operating conditions must be evaluated and if the process design involves multiple loops and requires iterative convergence of the reactor model at variable conditions. Although CFD provides a highly resolved hydrodynamic profile, its use in process design environments is often limited by this very high computational cost and the difficulty of integrating detailed chemical mechanisms.

In contrast, a reactor network model allows to reproduce the key hydrodynamic characteristics in a simplified way that can readily incorporate very complex detailed kinetics with negligible computational cost. This technique enables the investigation of a much broader

**Fig. 7.** The overall product yield comparison of Tran et al. and RN model at different temperatures.

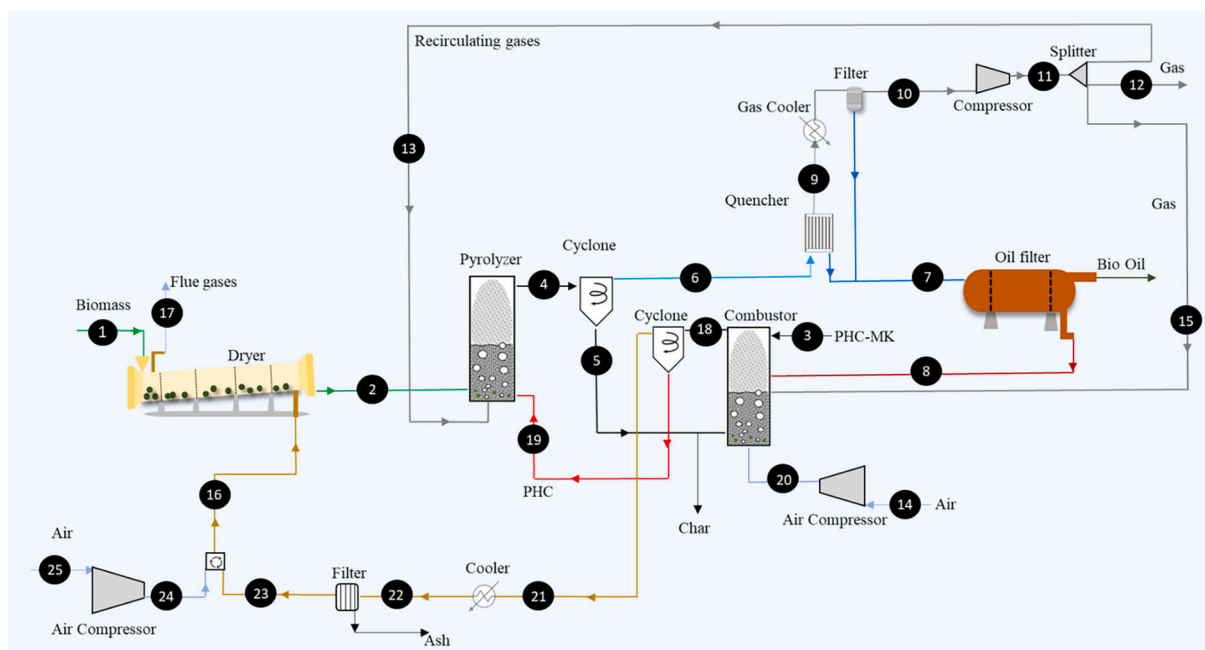


**Fig. 8.** Schematic diagram of the conventional pyrolysis process model [17].

range of chemical species under variable operating conditions, particularly help the analysis of secondary gas phase reactions and repolymerization phenomena that occur during the pyrolysis process. NetSMOKE, a tool based on the reactor network model, enables fast optimization, rapid sensitivity studies, and efficient convergence at variable operating conditions. These satisfactory results show the reliability and effectiveness of the tool of NetSMOKE when the experimental operational parameters are provided. Nevertheless, CFD models remain valuable for the initial development and validation of reactor network structures and for analyzing detailed flow and transport phenomena at high spatial resolution.

### 3. Pyrolysis process models

### 3.1. Conventional pyrolysis plant

The process model (Fig. 8) used in this study builds upon previously

published pyrolysis plant model [17], which is structured into five main sections: biomass pretreatment, pyrolysis, solids removal, bio-oil recovery, and combustion. The overall plant layout and operating principles remain consistent, with minor updates in biomass type and reactor temperature.

In the pretreatment section, biomass is dried using a direct rotary dryer, ensuring efficient pyrolysis. Hot gases for drying are obtained by blending flue gas from the combustor with ambient air, targeting an exit biomass moisture content to 10 %.

The pyrolysis is conducted in a fluidized bed reactor (FBR), with hot particles as heat carrier. In our previous work [17], the reactor was modeled as an RYield unit with a fixed yield distribution at 434°C. Here, we introduce a detailed reactor network model capable of handling variations in feedstock and operating conditions. Volatile products from reactor are separated from solids in a cyclone filter.

The bio-oil recovery section includes two-stage condensation followed by demisting and gas compression. Recovered bio-oil is filtered to

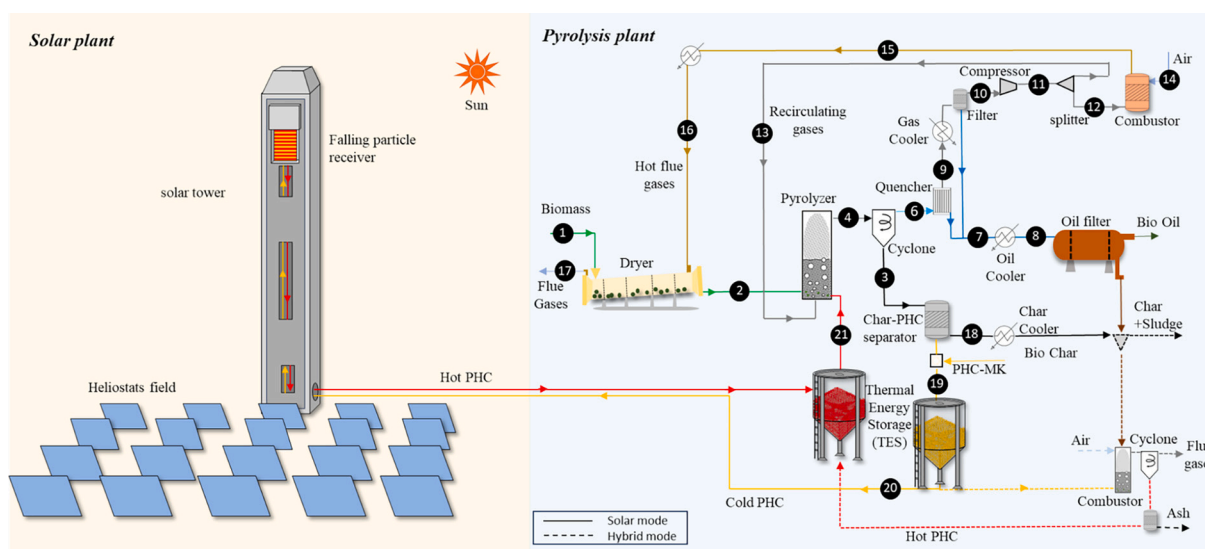


**Fig. 9.** Schematic diagram of CSP based pyrolysis process model [17].



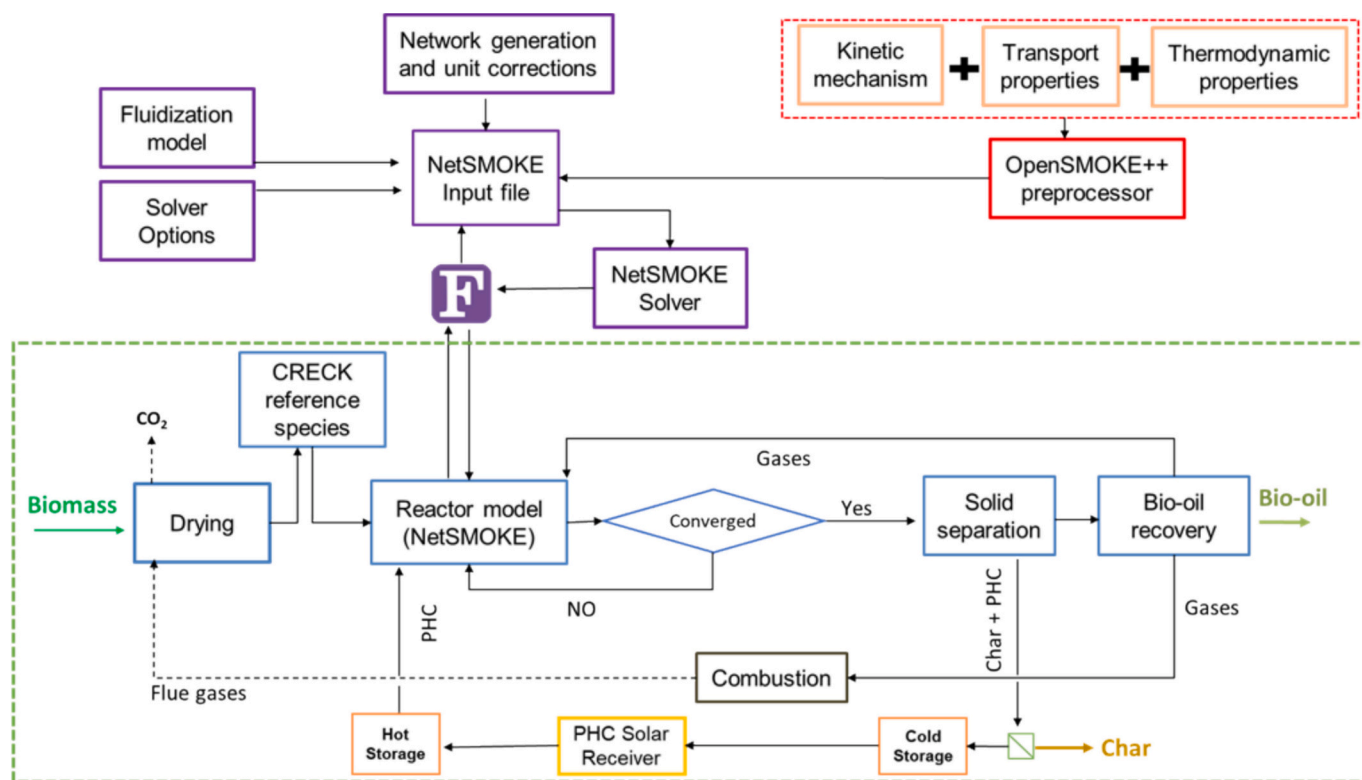


Fig. 10. Process flowsheet of solar driven biomass pyrolysis model of Aspen Plus®, integrated with reactor Model of NetSMOKE using Fortran subroutine.

remove entrained solids, with waste streams routed to the combustor. The combustor unit burns biochar, gas residues, and filter retentate to reheat the PHC. As biochar is a high-value product, a portion of the excess char can be retained if the generated heat is sufficient to reheat particle heat carrier (PHC) in combustor. Reheated PHC is reused in the FBR and hot flue gases are sent to the dryer. This process model adopts the same assumptions as outlined in our earlier work [17], to maintain consistency in methodology.

### 3.2. CSP based pyrolysis

To reduce the carbon footprint and energy demand of conventional pyrolysis, the combustor block is replaced by a Concentrated Solar Power (CSP) system, which supplies the necessary heat to the reactor. The solar integration allows recovery of biochar while avoiding CO<sub>2</sub>, NO<sub>x</sub>, and particulate emissions associated with combustion. Key modifications to the original setup [17] include:

- Replacing the combustor with a CSP unit;
- Adding a dedicated gas combustor for drying gases;
- Introducing a char recovery and cooling unit.

As shown in Fig. 9, solids from the pyrolyzer are first separated in a cyclone, then passed to a char-PHC separator. Char is recovered as a product, while PHC is recycled back to the CSP system, with an additional PHC makeup stream added to compensate for losses. Both recycled and makeup PHC are heated to approximately 200 °C higher than the operating temperature of pyrolyzer in the CSP unit. A separate combustor handles excess pyrolysis gases to produce hot drying air. These gases are cooled and mixed with air to ensure appropriate drying conditions without degrading biomass volatiles.

### 4. Integration of NetSMOKE with process model

The NetSMOKE tool can handle reactor configurations and complex

chemical kinetics, but it is unable to directly manage the mass and energy balances of the entire process due to the lack of auxiliary process model components. On the other side, a tool like Aspen Plus® process can do such analyses, but it lacks of a detailed description of the pyrolysis reactor performances. Integrating the RN tool into Aspen Plus® can potentially overcome the technical weaknesses of both.

To this aim, reactor network model is introduced in Aspen Plus® using a Fortran subroutine, which acts as an intermediary, receiving input data from Aspen Plus®, execute the NetSMOKE model with respect to provided data and return the detailed output data to the Aspen Plus® model.

As explained in previous study [17], the Aspen Plus® process model (section 3) uses RYield block to model reactor with fixed yield taken from literature, specific to biomass type at fixed operating conditions. The integration of the RN model with its accurate description of the complex kinetics involved in the pyrolysis makes the overall plant models (conventional and solar-assisted) more flexible and robust to tackle any biomass feedstock at variable operating conditions. Most importantly, it allows for a detailed and accurate description of both major products and minor or pollutant by-products. Two main modifications are needed in Aspen Plus® process model for an effective coupling of the two models:

1. A block is added to convert biomass elemental composition to CRECK reference species.
2. RYield reactor block is replaced by NetSMOKE solver linked by Fortran subroutine.

To accurately model biomass pyrolysis, the initial step involves proper characterization of the feedstock using elemental composition to CRECK reference species. In the Aspen Plus® model used in this study, biomass is introduced by defining its proximate and elemental composition. After passing through the dryer, the dried biomass is sent to the reactor for pyrolysis, but an additional user defined block is added in between to convert this biomass stream into CRECK reference species

**Table 6**

Biomass characterization of poplar wood obtained from CRECK-S-B model [wt %].

Ref. Species	wt%	Ref. Species	wt%	Ref. Species	wt%
CELL	0.3882	LIGH	0.0785	TGL	0.0332
GMSW	0.1775	LIGC	0.0837	Moisture	0.1000
LIGO	0.1016	TANN	0.0282	Ash	0.0092

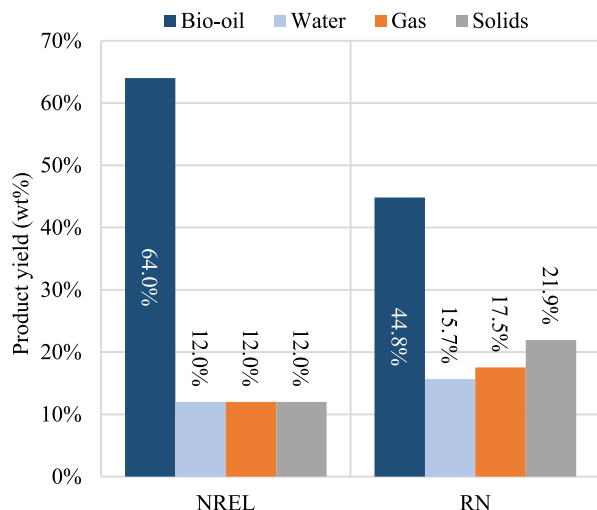


**Fig. 11.** Comparison of NREL-BM theoretical and RN-BM model driven product yield (wt%) at reactor outlet.

[27]. This upgrade is necessary to use the CRECK biomass kinetic model in NetSMOKE.

As shown in Fig. 10, the NetSMOKE solver is linked with another CRECK model (OpenSMOKE++) [50], which provides detailed chemical kinetics for the primary and secondary reactions of biomass pyrolysis, as well as thermodynamic and transport properties.

In the RN-integrated Aspen Plus® process model, the subroutine automatically generates the input file for the NetSMOKE solver based on the inlet stream data of reactor block. When the NetSMOKE solver runs, it processes this data to produce the output stream results, which are then passed back to the Aspen Plus® process model. If flue gases exiting the reactor are continuously recirculated to the reactor as a fluidization medium or if the PHC is recirculated in reactor, the inlet composition of RN model (NetSMOKE) block in process model changes, requiring iterations between NetSMOKE and Aspen Plus® until convergence on the outlet composition is reached. Apart from these two main changes in the process model, the rest of the process remains the same as previously used [17] and is briefly described in section 3. A detailed explanation and guide of how the Aspen Plus® program was integrated with NetSMOKE is provided in the supplementary information section S.2.

## 5. Application of RN model on pyrolysis process model

This integration of RN model enabled the process model to replace the yield values used in the National renewable energy laboratories (NREL) derived process model [51] that was based on fixed RYield reactor. The same RN model structure used in the first case study was adopted (section 2.3.1), with a reactor temperature of 434 °C and a total residence time of 2 s. The same process model used in the previous study [17] was adopted and the reactor model was integrated with the NetSMOKE reactor model.

To maintain consistency between both models, the biomass composition, thermodynamic stream properties, reactor operating conditions and inlet mass flows were kept the same (except outlet streams) as in the previous study [17]. In the beginning, the CRECK model converts dry

**Table 7**

Comparison of elemental composition for convention and CSP based pyrolysis models with respect to RN-BM and NREL-BM.

Product	Model type	Composition (% mass)					
		C	H	O	N	Ashes	PHC
Bio-oil	NREL-BM	41.6	7.8	50.6	0.0	–	–
	RN-BM	38.2	8.3	53.5	0.0	–	–
Char	NREL-BM	–	–	–	–	–	–
	RN-BM	71.8	4.5	17.8	–	4.1	1.7
Pyro-gas	NREL-BM	39.6	2.3	58.1	0.0	–	–
	RN-BM	36.9	3.0	60.1	0.0	–	–
Flue gases	NREL-BM	3.9	1.4	30.9	63.8	–	–
	RN-BM	4.8	2.0	32.8	59.4	–	–
Bio-oil	NREL-BM	41.6	7.8	50.6	0.0	–	–
	RN-BM	38.2	8.3	53.5	–	–	–
Char	NREL-BM	83.1	1.7	6.6	1.4	7.1	–
	RN-BM	72.6	4.6	18	–	4.2	0.6
Pyro-gas	NREL-BM	–	–	–	–	–	–
	RN-BM	36.9	3.0	60.1	–	–	–
Flue gases	NREL-BM	2.1	1.7	34.7	61.5	–	–
	RN-BM	1.6	1.9	35.2	60.2	–	–

biomass feed stream to CRECK reference species shown in Table 6.

The reference species data then transferred to reactor network block, which is seamlessly integrated to Aspen Plus® model. The yield composition obtained from reactor network-based process model is significantly different from those assumed in NREL based Aspen® process model under the same operating conditions. Results show that the liquid oil products are almost 20 percentage points higher in NREL model (Fig. 11) while water, gas and char are lower in NREL model with difference of almost 4–10 percentage points with respect to the reactor network-based model (RN-BM).

In the previous Aspen Plus® model, which is based on NREL data, the recirculating gas stream composition is fixed and it is difficult to predict its composition under the complex nature of pyrolysis process. This new model update also converged the gas composition of this recirculating stream under given operating conditions. The product elemental composition and carbon efficiency of the new RN-BM are compared with the NREL-BM model for both conventional pyrolysis and CSP-based systems in Table 7. Detailed stream results for the main inlet and outlet streams of process are provided in Supplementary Information (Section S.3). The primary difference lies in the change in the CHO composition of the oil and its carbon yield percentage (Table 7). In conventional pyrolysis model, the overall carbon yield of the oil (Fig. 12) decreased from 69 % to 51 %, with this reduction compensated by an increase in the production of char and pyrolysis gas during the process.

In the conventional pyrolysis process, the RN-BM shows a lower proportion of carbon yield in flue gases (22 %) compared to the NREL model (26 %), that means lower amount of CO<sub>2</sub> emissions (Fig. 12). In CSP based process model, the composition of char, oil, and pyro-gas, based on CHO analysis, changed significantly (Table 7). The % yield of carbon in char is significantly higher by almost 15.6 percentage points (Fig. 12), which can have advantages in terms of carbon management, especially when integrated with solar energy in the CSP-based system.

The biomass input (based on LHV) was kept constant at 10 MW in all cases, and in the CSP-based pyrolysis scenarios an additional 1.73 MW of solar heat was supplied, resulting in a higher overall power output compared with the conventional cases. On the other hand (Fig. 13), the power distribution at the process outlet indicates a decrease in the bio-oil contribution (sludge is here included in the bio-oil) by approximately 1.9–2.1 MW<sub>LHV</sub> in the RN-BM, primarily due to lower oil yields. Correspondingly, the share of char is higher in the RN-BM by about 1.3–1.7 MW<sub>LHV</sub>, reflecting increased char production. A slight increase in the gas share was also observed in RN-BM, attributed to marginally higher gas yields. Thermal losses associated with the sensible and latent heat of the product and of the flue gases, however, remained nearly

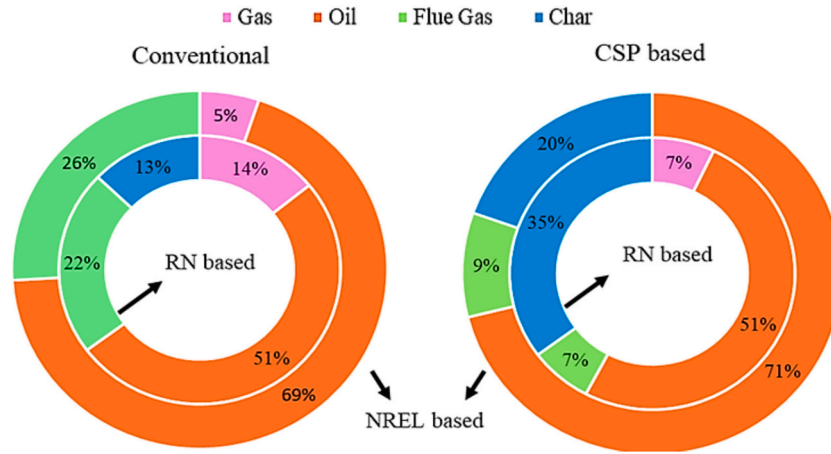


Fig. 12. Comparison of carbon distribution in process outlet streams in RN-BM (inner circle) and NREL-BM (outer circle) models. Sludge is considered as part of Bio-oil.

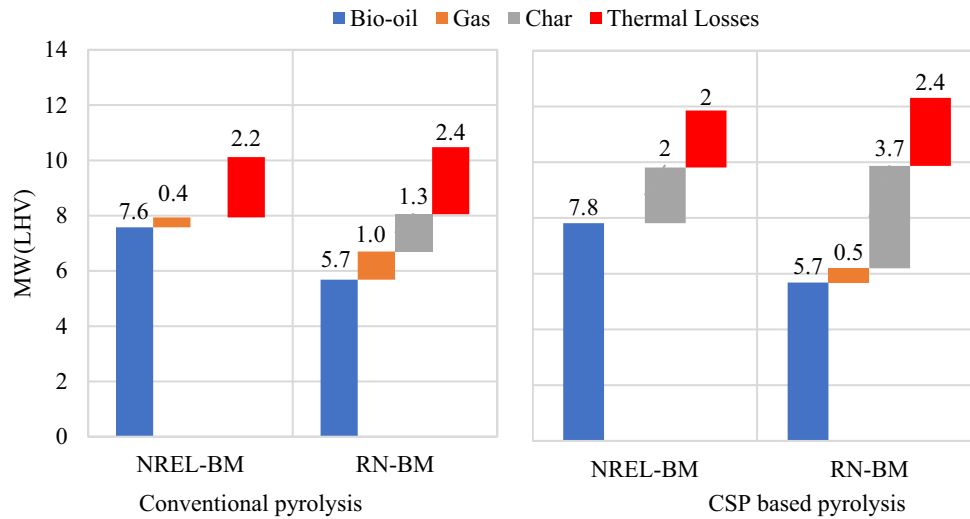


Fig. 13. Thermal power distribution comparison at process outlet in RN-BM and NREL-BM models. Sludge is considered as part of Bio-oil.

constant across both models, suggesting that the overall shift in power distribution results solely from variations in product yields. The detailed thermodynamic results of process model and energy balances are provided in S-Table 7.

### 5.1. Key performance indicators

Main key performance indicators assessed in previous study [17] are compared with RN-BM model. As demonstrated in the previous analysis, CSP-based pyrolysis plants outperform conventional systems not only in terms of energy efficiency but also with significantly lower emissions. When comparing the CO<sub>2</sub> emissions between the NREL-BM and RN-BM models, the RN-BM model exhibits lower emissions. This is primarily because it retains more char in product stream, and the majority of the carbon content remains stored in the char.

To compare the performances of the different configurations, two KPIs can be considered in accordance with [17]; i) the pyrolysis plant energy conversion efficiency  $\eta_{pyro-plant}$ , which is defined in Eq.(1) as the ratio between the products chemical energy (bio-oil, biochar, sludge) and the primary energy input, where  $\dot{m}_{prod,i}$  and  $LHV_i$  are the mass flowrate and the lower heating value of the  $i$ -th product,  $\dot{m}_{biom}$  is the biomass flowrate,  $P_{AUX}$  is the plant overall electric consumption,  $\eta_{el,ref}$  is the reference thermal to electrical energy efficiency (assumed equal to

50 %), and  $\dot{Q}_{PHC,pyro}$  is the thermal power provided via the PHC to the pyrolysis unit; ii) the carbon efficiency  $\varepsilon_C$ , which is defined in Eq.(2) as the ratio between the carbon contained in the useful products over the inlet carbon contained in biomass, where  $y_{C,prod,i}$  and  $y_{C,biom}$  are the carbon mass fractions of the  $i$ -th product and of biomass.

$$\eta_{pyro-plant} = \frac{\sum_i \dot{m}_{prod,i} \cdot LHV_{prod,i}}{\dot{m}_{biom} \cdot LHV_{biom} + \left( \frac{P_{AUX}}{\eta_{el,ref}} \right) + \dot{Q}_{PHC,pyro}} \quad (1)$$

$$\varepsilon_C = \frac{\sum_i \dot{m}_{prod,i} \cdot y_{C,prod,i}}{\dot{m}_{biom} \cdot y_{C,biom}} \quad (2)$$

Interestingly, despite the lower overall emissions, the emission-to-oil (ETO) ratio is slightly higher in the estimates of RN-BM model. This results from lower oil yield and the lower heating value of the produced oil, which leads to more emissions per unit of energy in the oil. However, the RN-BM model estimate higher carbon efficiency compared to the NREL-BM, due to its reduced CO<sub>2</sub> emissions. If the carbon is considered biogenic, the CSP-based cases show net negative ETO ratios of -27.5 kgCO<sub>2</sub>/Gj<sub>oil</sub> for the NREL-BM and -35.8 kgCO<sub>2</sub>/Gj<sub>oil</sub> for the RN-BM, highlighting their environmental potential in term of carbon capture. In case of energy conversion efficiency, the RN-BM model estimate higher efficiency in the conventional pyrolysis setup by utilizing both

**Table 8**

Key performance indicator comparison.

Model type	NREL Based Model		RN Based Model	
	Conventional	CSP based	Conventional	CSP based
CO <sub>2</sub> emissions (kt/y)	8.7	2.6	7.4	1.9
ETO ratio (kg <sub>CO2</sub> /GJ <sub>oil</sub> )	36.5	13.1	41.56	13.18
Net ETO ratio (kg <sub>CO2</sub> /GJ <sub>oil</sub> )	0	-27.5	0	-35.8
Carbon efficiency (%)	74.1	90.7	77.7	92.9
Energy conversion efficiency (%) $\eta_{pyro\ plant}$	73.9 %	78.6 %	75 %	77.7 %

char and oil as useful products. In the CSP-based scenario, however, the RN-BM exhibits slightly lower energy conversion efficiency than the NREL-BM, primarily due to marginally higher thermal losses. KPI

comparisons between the RN-based and NREL-based models are provided in Table 8.

## 6. Pyrolyzer temperature sensitivity analysis

To investigate the potential of the developed RN-BM pyrolysis model, a sensitivity analysis is carried out to understand how the mass and energy balances of the above-mentioned conventional and solar-based pyrolysis plants would change when varying the pyrolyzer outlet temperature  $T_{pyr}^{out}$ . Starting from both the plant configurations detailed in Section 3, the pyrolyzer outlet temperature is varied between 300 °C and 700 °C, keeping the  $\Delta T_{PHC}$  between hot PHC and pyrolyzer outlet temperature equal to 200 °C [51]. The PHC-to-biomass ratio increases from 9 to 18 according to the change in pyrolysis heat of reaction, while the fluidizing gas-to-biomass mass ratio is kept between 3 and 4 according to the previous study [51].

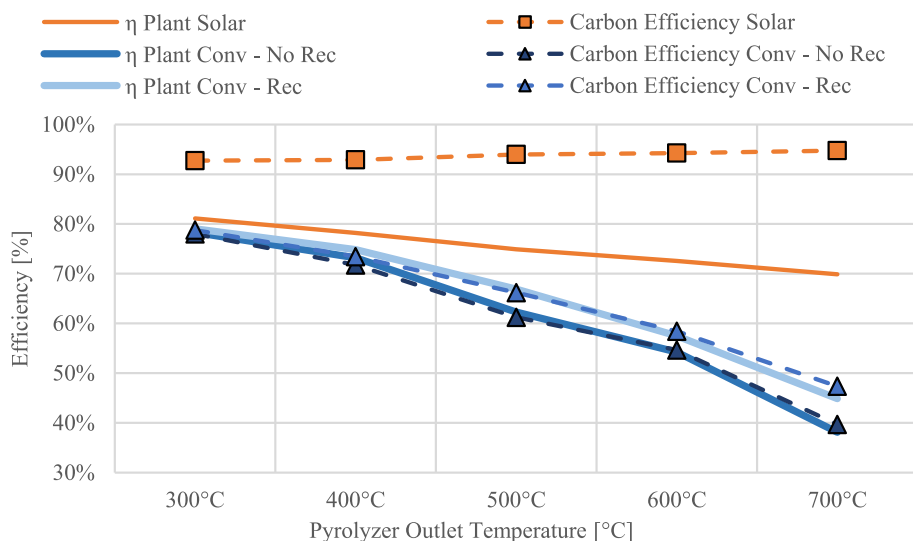


**Fig. 14.** Pyrolysis plant energy and carbon efficiencies for the conventional configuration, for the conventional configuration with a fraction of heat recovery from flue gases, and for the solar configuration.

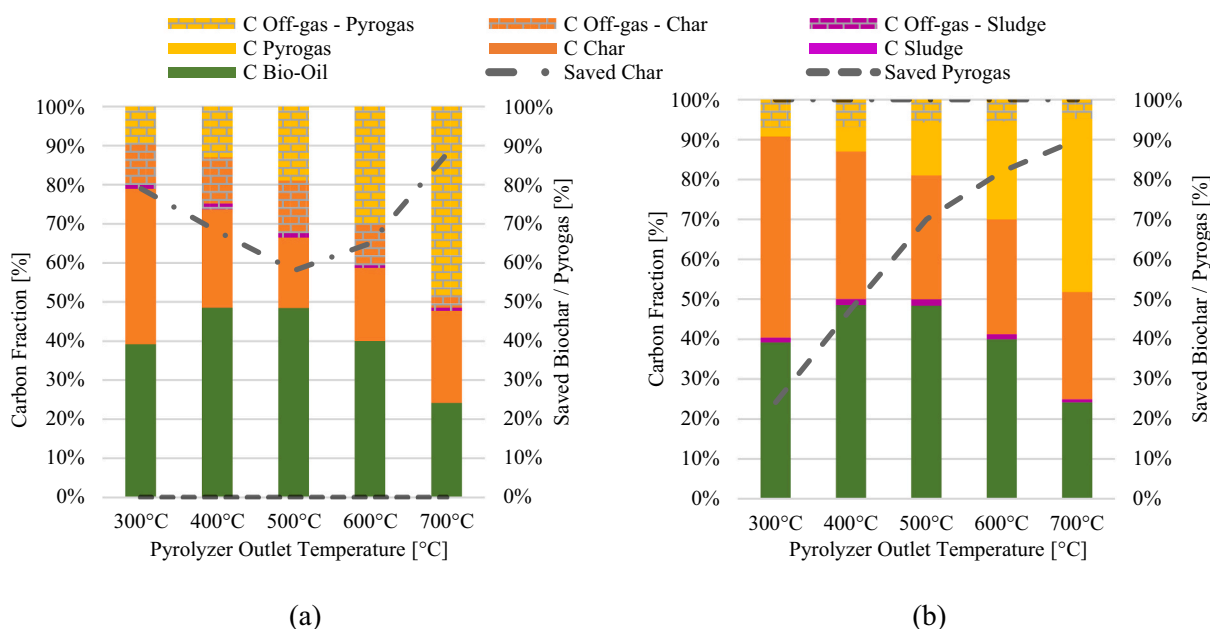


**Fig. 15.** a) Conventional and b) solar pyrolysis overall plant carbon balance and fraction of saved biochar and pyro-gas.



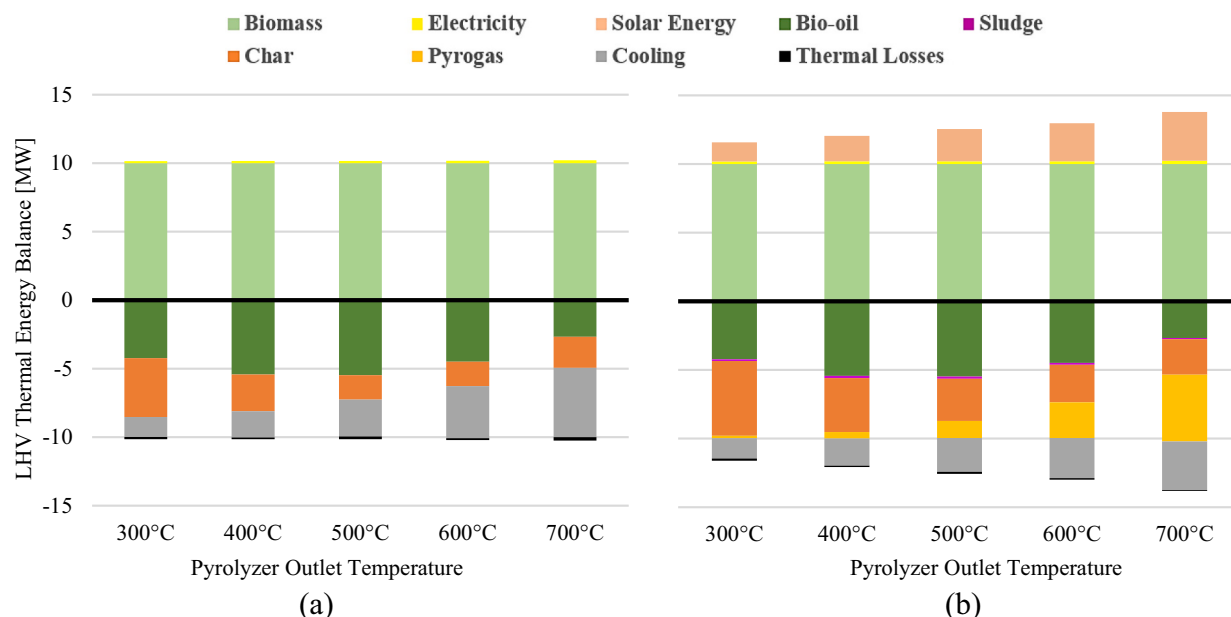


Fig. 16. a) conventional pyrolysis and b) solar based pyrolysis global LHV energy balance. The label “Solar Energy” is equivalent to  $\dot{Q}_{PHC,pyro}$ .

In the conventional plant, the main heat duties are related to the pyrolysis reactor  $\dot{Q}_{PHC,pyro}$  and to the dryer  $\dot{Q}_{dryer}$  and are satisfied through the combustion of sludge, char and pyrogas in the fluidized bed solid combustor. The combustor generates a hot PHC stream for the pyrolyzer and a hot flue gas stream for the dryer, both at  $T_{pyr}^{out} + \Delta T_{PHC}$ . The flue gases dryer inlet temperature is always kept lower than 350 °C to avoid unwanted early biomass decomposition reactions. In the solar-based plant, being  $\dot{Q}_{PHC,pyro}$  provided by solar energy,  $\dot{Q}_{dryer}$  is the only thermal load and is satisfied by burning a fraction of the pyrogas, which is mixed with enough air to maintain the dryer inlet temperature within the limit imposed.

The main results are illustrated in Fig. 14, featuring the pyrolysis plant efficiencies  $\eta_{pyro-plant}$  and the carbon efficiencies  $\varepsilon_C$  for both conventional and solar-based configurations. As can be seen, in the conventional case both  $\eta_{pyro-plant}$  and  $\varepsilon_C$  decrease when increasing  $T_{pyr}^{out}$  due to the increase of  $\dot{Q}_{PHC,pyro}$ , which increases the fraction of pyrolysis products (char, pyrogas and sludge) to be burned. Compared to the solar-based configuration, the conventional  $\eta_{pyro-plant}$  has a far steeper slope due to the working principle of the fluidized bed solid combustor, which in order to heat up the PHC at  $T_{pyr}^{out} + \Delta T_{PHC}$  it releases a stream of hot flue gases at the same temperature, thus generating a significant amount of high-temperature waste heat. If a partial recovery of this waste heat to pre-heat the air fed to the combustor up to 300 °C was considered, the efficiency decay will be reduced (light blue line in Fig. 14).

On the other hand, the solar-based  $\varepsilon_C$  slightly increases because, even though the dryer heat duty is constant varying  $T_{pyr}^{out}$ , the mass flowrate of combusted pyro-gas needed reduces due to the increase of pyro-gas LHV, which also increases the fraction of saved pyro-gas. These results can also be seen in Fig. 15 and Fig. 16, featuring the overall plant carbon and energy balances for both conventional and solar based configurations, respectively. In Fig. 15 the shaded area illustrates the carbon breakdown associated with the generation of off-gases, indicating which components (sludge, char, or pyrogas) were burned. In addition, the dashed and dash-dotted lines represent the fraction of pyrogas and char which weren't burned, respectively.

The mass loss of biomass begins between 120 °C and 200 °C due to drying, during this temperature range the thermal degradation of carbonaceous material is almost negligible. However, thermal

degradation starts around 200 °C. Initially, hemicellulose degrades, releasing light volatiles and CO<sub>2</sub>. From around 300 °C, cellulose also begins to decompose, and the production of liquid (bio-oil) and gaseous products increases significantly compared to the solid fraction (char). This trend continues up to about 500 °C, during which lignin gradually decomposes into volatiles and tars. The yield of liquid products tends to reach its maximum within this temperature range. However, above 500 °C, the liquid yield starts to decline because heavy oils and tars undergo secondary gas-phase reactions, forming lighter gases. Additionally, repolymerization reactions can lead to the formation of more solid (char-like) material.

As a result, the gas yield increases significantly at higher temperatures. Since the major decomposition of cellulose, hemicellulose, and lignin occurs below 500 °C, the char yield stabilizes above this temperature, with only a slight further decrease. This trend in product distribution (gas, liquid, solid) can be observed in Fig. 15 and CSP section of Fig. 16, and is also supported by previous studies [23,52] in the literature.

## 7. Conclusions

This study presents a significant advancement in the modeling of biomass pyrolysis by integrating a fully coupled, multiphase reactor network (NetSMOKE) tool with pyrolysis process model. Unlike many previous pyrolysis process models, this approach simultaneously captures the complex interactions among gas-phase reactions, solid devolatilization, and char conversion under varying operating conditions and feedstocks. This makes the model more realistic and better suited for predicting the behavior of different biomass feedstocks in diverse conditions.

The validation of the reactor model against both computational fluid dynamics (CFD) and experimental data demonstrates its robustness and predictive capability. The reactor network model achieves high accuracy during validation with only a 0.1–3.4 percentage points error margin. Importantly, this integrated approach allows for the analysis of detailed reaction pathways and intermediate species formation, which are often neglected in traditional process simulators. Such improvements directly support the optimization of pyrolysis reactor design and operation, particularly in fluidized bed systems where interdependent thermal, chemical, and hydrodynamic phenomena govern product

distribution and yield. Moreover, the incorporation of this reactor network model into a broader process simulation platform further enhances its practical utility. It helps to evaluate not only the reactor performance but also the energy efficiency, emissions, and overall process feasibility. The flexibility of this model makes it a valuable tool for designing better biomass conversion systems that are both efficient and environmentally friendly.

In the future, the reactor network model for pyrolysis could be further extended to incorporate auger reactors. Additionally, solid-particle heat carriers (PHC) and char separation, also require attention and should be both experimentally assessed and numerically modeled, as separation efficiency significantly influences biochar quality.

This novel technique bridges the gap between detailed chemical kinetics, reactor modeling, and process-level simulations. The proposed approach has the potential to accelerate the transition toward cleaner and more efficient renewable energy technologies.

#### CRediT authorship contribution statement

**Muhammad Ahsan Amjed:** Writing – original draft, Visualization, Validation, Software, Methodology, Formal analysis, Data curation, Conceptualization. **Marco Colombi:** Writing – original draft, Software, Formal analysis, Data curation. **Leon Loni Berkel:** Visualization, Methodology, Investigation. **Marco Binotti:** Writing – review & editing, Validation, Supervision, Project administration, Funding acquisition. **Matteo Carmelo Romano:** Writing – review & editing, Supervision. **Tiziano Faravelli:** Writing – review & editing, Supervision, Methodology, Funding acquisition.

#### Declaration of Generative AI and AI-assisted technologies in the writing process

Authors hereby declare that AI tools, such as ChatGPT and Gemini, were partially utilized solely for the purpose of refining the English language and readability in this manuscript. After using this tool/service, the authors reviewed and edited the content as needed and take full responsibility for the content of the publication. However, the content, ideas, methodology, results and analysis presented remain entirely by the authors.

#### Declaration of competing interest

The authors declare that they have no known competing financial interests or personal relationships that could have appeared to influence the work reported in this paper.

#### Acknowledgements



Funded by  
the European Union

This study is funded by the European Union under

Pysolo project (Grant Agreement n. 101118270). Views and opinions expressed are however those of the author(s) only and do not necessarily reflect those of the European Union or the European Climate, Infrastructure and Environment Executive Agency (CINEA). Neither the European Union nor the granting authority can be held responsible for them.

#### Appendix A. Supplementary data

Supplementary data to this article can be found online at <https://doi.org/10.1016/j.cej.2025.172206>.

#### Data availability

Data will be made available on request.

#### References

- [1] S.F. Javaid, M. Dai, Y. Wu, H. Luo, M.A. Amjed, I. Ali, C. Peng, I. Naz, Production of biochar by slow and solar-biomass pyrolysis: focus on the output configuration assessment, adaptability, and barriers to market penetration, *Arab. J. Sci. Eng.* 49 (2024) 7731–7750, <https://doi.org/10.1007/S13369-023-08549-3/TABLES/7>.
- [2] M. Antar, D. Lyu, M. Nazari, A. Shah, X. Zhou, D.L. Smith, Biomass for a sustainable bioeconomy: an overview of world biomass production and utilization, *Renew. Sust. Energ. Rev.* 139 (2021) 110691, <https://doi.org/10.1016/j.rser.2020.110691>.
- [3] M.A. Amjed, C. Peng, M. Dai, Q. Chang, I. Ali, M. Sultan, I. Naz, M.U. K. Muhammad Z Farooq, Muhammad Kashif, Recent updates on the solar-assisted biochar production and potential usage for water treatment, *Fresenius Environ. Bull.* 29 (2020) 5616–5632.
- [4] K. Zeng, D. Gauthier, J. Soria, G. Mazza, G. Flamant, Solar pyrolysis of carbonaceous feedstocks : a review, *Sol. Energy* 156 (2017) 73–92, <https://doi.org/10.1016/j.solener.2017.05.033>.
- [5] K. Zeng, D.P. Minh, D. Gauthier, E. Weiss-Hortala, A. Nzihou, G. Flamant, The effect of temperature and heating rate on char properties obtained from solar pyrolysis of beech wood, *Bioresour. Technol.* 182 (2015) 114–119, <https://doi.org/10.1016/j.biortech.2015.01.112>.
- [6] J. Yu, S. Shan, S. Liu, Z. Zhou, Z. Wang, K. Cen, Experimental study on the gasification characteristics of biomass pyrolysis semi-coke driven by concentrated solar energy, *Chem. Eng. J.* (2025) 168222, <https://doi.org/10.1016/j.cej.2025.168222>.
- [7] V. Chintala, S. Kumar, J.K. Pandey, Assessment of performance, combustion and emission characteristics of a direct injection diesel engine with solar driven Jatropa biomass pyrolysed oil, *Energy Convers. Manag.* 148 (2017) 611–622, <https://doi.org/10.1016/j.enconman.2017.05.043>.
- [8] M.A. Amjed, X. Wu, I. Ali, I. Naz, M. Dai, A. Tehrim, W. Niaz, S.F. Javaid, C. Peng, Surface decoration and characterization of solar driven biochar for the removal of toxic aromatic pollutant, *J. Chem. Technol. Biotechnol.* 96 (2021) 2310–2324, <https://doi.org/10.1002/jctb.6759>.
- [9] V. Chintala, Production, upgradation and utilization of solar assisted pyrolysis fuels from biomass – a technical review, *Renew. Sust. Energ. Rev.* 90 (2018) 120–130, <https://doi.org/10.1016/j.rser.2018.03.066>.
- [10] H. Wu, D. Gauthier, Y. Yu, X. Gao, G. Flamant, Solar-thermal pyrolysis of Mallee wood at high temperatures, *Energy Fuel* 32 (2018) 4350–4356, <https://doi.org/10.1021/acs.energyfuels.7b03091>.
- [11] Y. Xie, K. Zeng, G. Flamant, H. Yang, N. Liu, X. He, X. Yang, A. Nzihou, H. Chen, Solar pyrolysis of cotton stalk in molten salt for bio-fuel production, *Energy* 179 (2019) 1124–1132, <https://doi.org/10.1016/j.energy.2019.05.055>.
- [12] J. Li, J. Peng, K. Zeng, D. Zhong, K. Xu, V.S. Vladimirovich, A. Nzihou, H. Yang, H. Chen, Solar pyrolysis of algae in molten salt for capacitive carbon preparation, *J. Clean. Prod.* 406 (2023) 136898, <https://doi.org/10.1016/j.jclepro.2023.136898>.
- [13] R. Adinberg, M. Epstein, J. Karni, Solar gasification of biomass: a molten salt pyrolysis study, *Journal of Solar Energy Engineering, Transactions of the ASME* 126 (2004) 850–857, <https://doi.org/10.1115/1.1753577>.
- [14] C. Zheng, K. Cheng, D. Han, High-temperature molten salt heat exchanger technology: research advances, challenges, and future perspectives, *Energies* 18 (2025), <https://doi.org/10.3390/EN18123195>, Page 3195 18 (2025) 3195.
- [15] Y. Shen, X. Yuan, Research advancement in molten salt-mediated thermochemical upcycling of biomass waste, *Green Chem.* 25 (2023) 2087–2108, <https://doi.org/10.1039/d2gc04872h>.
- [16] Pysolo Project, (n.d.). <https://pysolo.eu/> (accessed October 20, 2023).
- [17] M.A. Amjed, Filip Sobic, M.C. Romano, Tiziano Faravelli, Marco Binotti, Techno-economic analysis of a solar-driven biomass pyrolysis plant for bio-oil and biochar production, *Sustain. Energy Fuels* (2024), <https://doi.org/10.1039/D4SE00450G>.
- [18] P. Kaushal, T. Pröll, H. Hofbauer, Model for biomass char combustion in the riser of a dual fluidized bed gasification unit: part 1 — model development and sensitivity analysis, *Fuel Process. Technol.* 89 (2008) 651–659, <https://doi.org/10.1016/J.FUPROC.2007.12.010>.
- [19] K. Onarheim, Y. Solantausta, J. Lehto, Process simulation development of fast pyrolysis of wood using Aspen plus, *Energy Fuel* 29 (2015) 205–217, [https://doi.org/10.1021/EF502023Y/ASSET/IMAGES/LARGE/EF-2014-02023Y\\_0017.JPEG](https://doi.org/10.1021/EF502023Y/ASSET/IMAGES/LARGE/EF-2014-02023Y_0017.JPEG).
- [20] D. Han, X. Yang, R. Li, Y. Wu, Environmental impact comparison of typical and resource-efficient biomass fast pyrolysis systems based on LCA and Aspen plus simulation, *J. Clean. Prod.* 231 (2019) 254–267, <https://doi.org/10.1016/J.JCLEPRO.2019.05.094>.
- [21] J.F. Peters, S.W. Banks, A.V. Bridgwater, J. Dufour, A kinetic reaction model for biomass pyrolysis processes in Aspen plus, *Appl. Energy* 188 (2017) 595–603, <https://doi.org/10.1016/J.APENERGY.2016.12.030>.
- [22] R. Toonssen, N. Woudstra, A.H.M. Verkooijen, Exergy analysis of hydrogen production plants based on biomass gasification, *Int. J. Hydrog. Energy* 33 (2008) 4074–4082, <https://doi.org/10.1016/J.IJHYDENE.2008.05.059>.
- [23] D. Meier, B. Van De Beld, A.V. Bridgwater, D.C. Elliott, A. Oasmaa, F. Preto, State-of-the-art of fast pyrolysis in IEA bioenergy member countries, *Renew. Sust. Energ. Rev.* 20 (2013) 619–641, <https://doi.org/10.1016/J.RSER.2012.11.061>.

- [24] D. Pallarès, F. Johnsson, Modeling of fluidized bed combustion processes, *Fluidized Bed Technologies for Near-Zero Emission Combustion and Gasification* (2013) 524–578, <https://doi.org/10.1533/9780857098801.2.524>.
- [25] Z. Kaczor, Z. Buliński, S. Werle, Modelling approaches to waste biomass pyrolysis: a review, *Renew. Energy* 159 (2020) 427–443, <https://doi.org/10.1016/j.renene.2020.05.110>.
- [26] H. Fatehi, X.S. Bai, A comprehensive mathematical model for biomass combustion, *Combust. Sci. Technol.* 186 (2014) 574–593, <https://doi.org/10.1080/00102202.2014.883255>.
- [27] E. Ranzi, P.E.A. Debiagi, A. Frassoldati, Mathematical modeling of fast biomass pyrolysis and bio-oil formation. Note I: kinetic mechanism of biomass pyrolysis, *ACS Sustain. Chem. Eng.* 5 (2017) 2867–2881, <https://doi.org/10.1021/acssuschemeng.6b03096>.
- [28] M. Trninić, D. Stojiljković, N. Manić, Ø. Skreiberg, L. Wang, A. Jovović, A mathematical model of biomass downdraft gasification with an integrated pyrolysis model, *Fuel* 265 (2020) 116867, <https://doi.org/10.1016/j.fuel.2019.116867>.
- [29] B. Hooshdaran, M. Haghsheenasfard, S.H. Hosseini, M.N. Esfahany, G. Lopez, M. Olazar, CFD modeling and experimental validation of biomass fast pyrolysis in a conical spouted bed reactor, *J. Anal. Appl. Pyrolysis* 154 (2021) 105011, <https://doi.org/10.1016/j.jaap.2020.105011>.
- [30] Q. Xue, D. Dalluge, T.J. Heindel, R.O. Fox, R.C. Brown, Experimental validation and CFD modeling study of biomass fast pyrolysis in fluidized-bed reactors, *Fuel* 97 (2012) 757–769, <https://doi.org/10.1016/j.fuel.2012.02.065>.
- [31] X. Yu, P.H. Blanco, Y. Makkawi, A.V. Bridgwater, CFD and experimental studies on a circulating fluidised bed reactor for biomass gasification, *Chem. Eng. Process. Process Intensif.* 130 (2018) 284–295, <https://doi.org/10.1016/j.cep.2018.06.018>.
- [32] K. Ehrhardt, M. Toqan, P. Jansohn, J.D. Teare, J.M. Beér, G. Sybon, W. Leuckel, Modeling of NO<sub>x</sub> reburning in a pilot scale furnace using detailed reaction kinetics, *Combust. Sci. Technol.* 131 (1998) 131–146, <https://doi.org/10.1080/00102209808935758>.
- [33] M. Falcitelli, L. Tognotti, S. Pasini, An algorithm for extracting chemical reactor network models from CFD simulation of industrial combustion systems, *Combust. Sci. Technol.* 174 (2002) 27–42, <https://doi.org/10.1080/713712951>.
- [34] S. Trespi, H. Nicolai, P. Debiagi, J. Janicka, A. Dreizler, C. Hasse, T. Faravelli, Development and application of an efficient chemical reactor network model for oxy-fuel combustion, *Energy Fuel* 35 (2021) 7121–7132, <https://doi.org/10.1021/acs.energyfuels.0c03560>.
- [35] J. Darido, A. Dhahak, R. Bounaceur, C. Le Dreff - Lorimier, G. Leyssens, F. Cazier, P. Genevray, F. Battin-Leclerc, Emissions from a domestic wood heating appliance: experimental measurements and numerical study using an equivalent reactor network (ERN) approach coupled with a detailed chemical mechanism, *Energy Fuel* 35 (2021) 18680–18698, <https://doi.org/10.1021/acs.energyfuels.1c01927>.
- [36] B. Das, A. Bhattacharya, A. Datta, Kinetic modeling of biomass gasification and tar formation in a fluidized bed gasifier using equivalent reactor network (ERN), *Fuel* 280 (2020), <https://doi.org/10.1016/j.fuel.2020.118582>.
- [37] A.K. Stark, C. Altantzis, R.B. Bates, A.F. Ghoniem, Towards an advanced reactor network modeling framework for fluidized bed biomass gasification: incorporating information from detailed CFD simulations, *Chem. Eng. J.* 303 (2016) 409–424, <https://doi.org/10.1016/j.cej.2016.06.026>.
- [38] L.L. Berkel, P. Debiagi, H. Nicolai, M.A. Amjed, A. Stagni, C. Hasse, T. Faravelli, Development of a multiphase chemical reactor network method as a tool for simulating biomass gasification in fluidized beds, *Fuel* 357 (2024), <https://doi.org/10.1016/j.fuel.2023.129731>.
- [39] E. Ranzi, A. Cuoci, T. Faravelli, A. Frassoldati, G. Migliavacca, S. Pierucci, S. Sommariva, Chemical kinetics of biomass pyrolysis, *Energy Fuel* 22 (2008) 4292–4300, <https://doi.org/10.1021/ef800551t>.
- [40] P.E.A. Debiagi, C. Pecchi, G. Gentile, A. Frassoldati, A. Cuoci, T. Faravelli, E. Ranzi, Extractives extend the applicability of multistep kinetic scheme of biomass pyrolysis, *Energy Fuel* 29 (2015) 6544–6555, <https://doi.org/10.1021/acs.energyfuels.5b01753>.
- [41] P. Debiagi, G. Gentile, A. Cuoci, A. Frassoldati, E. Ranzi, T. Faravelli, A predictive model of biochar formation and characterization, *J. Anal. Appl. Pyrolysis* 134 (2018) 326–335, <https://doi.org/10.1016/j.jaap.2018.06.022>.
- [42] X. Zou, P. Debiagi, M.A. Amjed, M. Zhai, T. Faravelli, Impact of high-temperature biomass pyrolysis on biochar formation and composition, *J. Anal. Appl. Pyrolysis* 179 (2024) 106463, <https://doi.org/10.1016/J.JAAP.2024.106463>.
- [43] L. Lu, X. Gao, A. Gel, G.M. Wiggins, M. Crowley, B. Pecha, M. Shahnam, W. A. Rogers, J. Parks, P.N. Ciesielski, Investigating biomass composition and size effects on fast pyrolysis using global sensitivity analysis and CFD simulations, *Chem. Eng. J.* 421 (2021) 127789, <https://doi.org/10.1016/j.cej.2020.127789>.
- [44] CRECKmodelling kinetic Mechanism, (n.d.). <https://github.com/CRECKMODELING/Kinetic-Mechanisms>.
- [45] J.F. Davidson, D. Harrison, J.R.F. Guedes de Carvalho, On the liquidlike behavior of fluidized beds, *Annu. Rev. Fluid Mech.* 9 (1997) 55–86.
- [46] C.T. Crowe, *Multiphase flow handbook*, CRC Press, 2005, <https://doi.org/10.1201/9781420040470>.
- [47] R.P.F. Bates, B. Richard, Ahmed F. Ghoniem, Whitney S. Jablonski, Daniel L. Carpenter, Christos Altantzis, Aaron Garg, John L. Barton, Ran Chen, Steam-air blown bubbling fluidized bed biomass gasification BFBBG multi-scale models and experimental validation, *AIChE J.* 63 (2017) 1543–1565.
- [48] L. Lu, M. Brennan Pecha, G.M. Wiggins, Y. Xu, X. Gao, B. Hughes, M. Shahnam, W. A. Rogers, D. Carpenter, J.E. Parks, Multiscale CFD simulation of biomass fast pyrolysis with a machine learning derived intra-particle model and detailed pyrolysis kinetics, *Chem. Eng. J.* 431 (2022) 133853, <https://doi.org/10.1016/j.cej.2021.133853>.
- [49] Q.K. Tran, M.L. Le, H.V. Ly, H.C. Woo, J. Kim, S.S. Kim, Fast pyrolysis of pitch pine biomass in a bubbling fluidized-bed reactor for bio-oil production, *J. Ind. Eng. Chem.* 98 (2021) 168–179, <https://doi.org/10.1016/j.jiec.2021.04.005>.
- [50] A. Cuoci, A. Frassoldati, T. Faravelli, E. Ranzi, OpenSMOKE++: an object-oriented framework for the numerical modeling of reactive systems with detailed kinetic mechanisms, *Comput. Phys. Commun.* 192 (2015) 237–264, <https://doi.org/10.1016/J.CPC.2015.02.014>.
- [51] S. Jones, P. Meyer, L. Snowden-Swan, K.J. Susanne, M. Pimphan, Snowden-SwanLesley, P. Asanga, T. Eric, D. Abhijit, J. Jacob, Cafferty, S. Jones, P. Meyer, L. Snowden-Swan, *Process Design and Economics for the Conversion of Lignocellulosic Biomass to Hydrocarbon Fuels: Fast Pyrolysis and Hydrotreating Bio-Oil Pathway*, 2013.
- [52] S. Şensöz, M. Can, Pyrolysis of pine (*Pinus Brutia* ten.) chips: 1. Effect of pyrolysis temperature and heating rate on the product yields, *Energy Sources* 24 (2002) 347–355, <https://doi.org/10.1080/00908310252888727>.